PADI4-mediated citrullination of histone H3 stimulates HIV-1 transcription

Luca Love[1,*], Bianca B Jütte[1,*], Birgitta Lindqvist[1], Hannah Rohdjess[1], Oscar Kieri[2,3], Piotr Nowak[2,3], J Peter Svensson[1]

[1] Division of Biosciences and Nutrition, Department of Medicine Huddinge, Karolinska Institutet, Huddinge, Sweden

[2] Department of Infectious Diseases, Karolinska University Hospital, Stockholm, Sweden

[3] Division of Infectious Diseases, Department of Medicine Huddinge, Karolinska Institutet, Huddinge, Sweden

*These authors contributed equally

Correspondence to JPS (peter.svensson@ki.se)

Highlights:

- The PADI4 enzyme stimulates HIV-1 transcription during T cell activation.
- PADI4 citrullinates histone H3 at the HIV-1 promoter upon T cell activation and inhibiting PADI4 reduces HIV-1 reactivation in *ex vivo* CD4 T cells from people living with HIV-1.
- H3cit is mostly found at gene promoters, and productive HIV-1 proviruses are more likely than latent or reactivatable proviruses, to integrate in chromatin susceptible for citrullination.
- H3cit inhibits latency establishment by interfering with the binding of HP1α to H3K9me3, preventing heterochromatin formation.

Abstract

HIV-1 infection establishes a reservoir of long-lived cells with integrated proviral DNA that can persist despite antiretroviral therapy (ART). Some of these reservoir cells can at anytime be reactivated and reinitiate infection. The mechanisms governing proviral latency the transcriptional regulation of the provirus are complex and have not yet been sufficiently described. Here, we identified a role for histone H3 citrullination, a post-translational modification catalyzed by protein-arginine deiminase type-4 (PADI4), in HIV-1 transcription and latency. We found that PADI4 inhibition by GSK484 reduced HIV-1 transcription after T cell activation in *ex vivo* cultures of CD4 T cells from people living with HIV-1 (PLWH). The effect was more pronounced in individuals with active viremia compared to individuals with effective ART . Using cell models of HIV-1 latency, we showed that PADI4-mediated citrullination of histone H3 occurred at the HIV-1 promoter upon T cell stimulation which facilitated proviral transcription. HIV-1 preferentially integrated into genomic regions marked by H3 citrullination and these integrated proviruses were less prone to latency compared to those in non-citrullinated chromatin. Inhibiting PADI4 led to compaction of the HIV-1 promoter chromatin and an increase of HP1α-covered heterochromatin, in a mechanism partly dependent on the HUSH complex. Our data reveal a novel mechanism to explain HIV-1 latency and transcriptional regulation.

Introduction

HIV-1 establishes a latent viral reservoir that persists despite active antiretroviral therapy (ART). The cells in the latent reservoir represent a heterogeneous population in different T cell subsets. Even though the cells in the latent reservoir do not produce viral particles, the HIV-1 provirus can still be transcriptionally active [1–3]. In other cells, the provirus is likely to be permanently silent, such as those integrated in epigenetically silent regions [4–6]. Before the start of ART, HIV-1 gradually depletes the CD4 T cell population. However, once ART is initiated, latently infected cells are selected for, since the host immune system eliminates cells expressing viral epitopes [7]. Some of these latent cells can switch between silent and active states of the provirus to avoid detection by the immune system, thus maintaining the ability to re-initiate active infection if ART is interrupted. Latency can be induced by many factors (reviewed in [8]), but a key determinant in long term latency is the chromatin constitution of the provirus [5,6]. As HIV-1 enters the genome, it is assumed to take the epigenetic profile of the chromatin where it integrates. However, the host cell can stably silence a locus through different mechanisms including the KRAB-ZFP (KAP1) transcription factor and Human Silencing Hub (HUSH) [9] leading to heterochromatin protein 1 (HP1) deposition over the provirus [10,11]. A more transient proviral inactivation is provided by lysine deacetylations [12].

The proviral sequence resembles a host gene in several aspects, and the resulting transcripts are initially processed similarly to human mRNAs. However, at the stage of virus production, the

59 spliceosome is turned off and the unspliced viral RNA genome is transcribed to be packaged into virions
60 [13]. It is unclear what promotes this switch, but acetylation of viral transactivator protein Tat has been
61 proposed as one mechanism leading to loss of splicing [14]. Unspliced transcripts are recognized as
62 foreign by the HUSH complex, and specifically the TASOR subunit. This recognition initiates a process
63 of silencing the chromatin whereby the histone H3 lys9 is methylated (H3K9me3) to enable
64 heterochromatin [15].
65 A chromatin modification that has been associated with preventing silencing of foreign DNA [16], yet not
66 studied from the perspective of HIV-1, is histone citrullination. Histone citrullination affects the
67 compaction of nucleosomes [17], thereby affecting chromatin accessibility of promoters [18]. These
68 changes in chromatin accessibility have been attributed to the reduced electrostatic attraction
69 between histones and DNA when positively charged arginine is converted to neutral citrulline [17].
70 Histone modifications serve as a platform for the binding of other proteins. H3K9me3 is recognized
71 and bound by the chromodomain of the α variant of HP1 (HP1α) [19]. Modification of arginine adjacent
72 to lysine residues can affect the binding of chromodomain proteins that recognize methylated lysines
73 [16]. Arginines can be modified by methylation or citrullination [20]. Citrullination is mediated by members
74 of the protein-arginine deiminase (PADI) family, of which PADI2 and PADI4 are found in the nucleus
75 and have partially redundant functionality [21]. PADI4 is an enzyme primarily expressed in less
76 differentiated cells and various cancer cells [22–25]. It citrullinates targets in the cell nucleus, including
77 several residues of histone H1, histone H3 and HP1γ [25–27]. H3cit8 interferes with HP1α-binding to
78 H3K9me3 in the process of regulating human endogenous retroviruses (HERVs) [16].
79 Here we describe a PADI4-mediated citrullination effect on HIV-1 transcription and latency reversal.
80 *De novo* histone H3 citrullination accompanies HIV-1 transcription during cell activation and prevents
81 proviral latency establishment, especially before ART is initiated. PADI4 acts partly through H3R8cit
82 that interferes with HIV-1 latency initiation by interfering with the binding of HP1α to H3K9me3,
83 preventing heterochromatin formation at the HIV-1 promoter.
84

85 ## Results

86 **PADI4 stimulates HIV-1 transcription after cell stimulation in cells from viremic ART naïve people**
87 **with HIV-1**

88 To test the hypothesis that citrullination affects the latent HIV-1 provirus in reservoir cells from PLWH,
89 we recruited 31 study participants to a clinical study. Given the known effect of PADI4-mediated
90 histone citrullination on heterochromatin [16,25] together with the observation that the reservoir of intact
91 proviruses becomes heterochromatic with time [6,28], we included two groups in our cohort. Firstly,
92 viremic study participants (n=14) and secondly, participants with long-term (>6 years) ART suppressed
93 viremia (<50c/ml) (n=17). The study participants were matched across various characteristics, apart

94 from their plasma viremia levels and ART status (Table S1). CD4 T cells were isolated from peripheral
95 blood. The cells were activated by phorbol-12-myristate-13-acetate and ionomycin (PMAi) after
96 treatment with PADI4 inhibitor GSK484 or mock treatment. The intact HIV-1 reservoir was measured
97 using Intact proviral DNA assay (IPDA) [29]. Cell-free RNA was measured by the amount of intact virus
98 RNA in the supernatant [30]. For cell-associated RNA, the LTR region and the multiply spliced RNA was
99 investigated.
100 In the entire cohort, GSK484 reduced the *ex vivo* HIV-1 activation based on cell-free RNA (Fig 1A). RNA
101 data could be obtained from 21 study participants (viremic: n=9, ART: n=12). Stratification between
102 viremic and ART suppressed study participants showed that cell activation induced a release of intact
103 viral particles only in cells from viremic study participants. The virus release was dependant on PADI4
104 as it was abolished in cells treated with GSK484. Activation of cells from the ART treated study
105 participants did not result in release of intact viruses (Fig 1B). This difference was not a consequence
106 of different numbers of infected cell as the intact HIV-1 reservoir was similar between the two groups
107 (Fig 1C). We continued to investigate the RNA prior to viral release. The cell-associated RNA from the
108 LTR transcripts showed that both groups had a clear proviral activation after PMAi-stimulation (Fig 1D).
109 This increase of LTR transcripts was not significant in the presence of GSK484. A comparison between
110 PMAi-stimulated cells showed a significant reduction in viremic samples pre-exposed to GSK484 (Fig
111 1D). Multiply spliced processed RNA (Tat-Rev) was induced by PMAi activation in cells from ART
112 suppressed study participants only (Fig 1E), implying involvement of Tat in the latency reversal process
113 in this group. A lack of mRNAs encoding Tat in activated cells from viremic study participants suggests
114 that latency reversal in these cells was Tat-independent or that the Tat protein was already present in
115 these cells. As the effect of GSK484 was most strongly associated with viremic study participants, we
116 quantitated the levels of *PADI4* to determine if the differences could be attributed to different protein
117 amounts. We observed that the expression of *PADI4* varied considerably in the cohort, but there was
118 no difference between *PADI4* expression in resting CD4 T cells from viremic or ART suppressed study
119 participants (Fig 1F).
120 This data show that PADI4 influences HIV-1 latency reversal in cells from people living with HIV-1,
121 particularly before the initiation of ART.
122
123 **PADI4 facilitates HIV-1 transcription after cell stimulation in cell models**
124 To investigate mechanisms underlying the effects of PADI4 inhibition on HIV-1 proviral activation, we
125 used established cell models of HIV-1 latency. The J-lat clone 5A8 is a Jurkat-derived cell line with a
126 single copy of a reporter HIV-1 integrated in an intron of the *MAT2A* locus. Proviral expression can be
127 tracked by flow cytometry or microscopy as the sequence for *nef* is replaced by *gfp* [31,32]. To test the

128 selectivity of PADI enzymes for the effect on HIV-1 transcription, cells were exposed to three different
129 PADI inhibitors: pan-PADI inhibitor Cl-amidine, PADI2-specific CAY10723, and PADI4-specific GSK484.
130 The effect was measured by flow cytometry after 24 h exposure. The PADI inhibitors alone had no
131 effect on HIV-1 latency reversal (Fig 2A). When cells were exposed to PADI inhibitors in combination
132 with PMAi to stimulate the cells, Cl-amidine and especially GSK484 resulted fewer GFP-positive cells
133 (Fig 2A). We also compared the effect of GSK484 with GSK106, an inactive control of GSK484, showing
134 that GSK484 reduces the level of HIV-1 reactivation compared to GSK106 (Fig S1). This suggests that
135 citrullination by PADI4 is part of a HIV-1 latency reversal mechanism. CAY10723 resulted in no
136 significant decrease in HIV reactivation when the cells were activated with PMAi. PADI4 is known to be
137 expressed in neutrophils [33], but the gene is also weakly expressed in many other cell types. In our cells,
138 we verified that PADI4 was expressed, although at low basal level (Fig 2B) (1,700 copies/10 ng RNA).
139 Upon cell stimulation, PADI4 expression was increased (Fig 2B). To understand the kinetics of the
140 GSK484 effect, we set up a time course experiment and observed that the PADI4 inhibition led to a
141 lower plateau of proviral activation although the kinetics of latency reversal were similar (Fig 2C). This
142 is consistent with a subpopulation of cells being affected by PADI4 inhibition. To test if the short
143 GSK484 half-life postpones activation, we also performed a pulse experiment with PMAi and GSK484
144 present for one hour and then washed out. The results were similar between a pulse or continuous
145 exposure indicating that the effect we observed is induced in the first hour of activation, at the early
146 stages of HIV latency reversal (Fig 2C).
147 In the nucleus, PADI4 citrullinates many targets, including histone H3. As observed previously [16], global
148 H3cit was induced within an hour after cell activation as measured by immunoblot. This induction is
149 not observed after PADI4 inhibition (Fig 2D). As expected from the stable nature of the H3cit
150 modification, GSK484 prevents *de novo* citrullination but it does not reduce H3cit in a short time period
151 (Fig 2D).
152 Stimulating T cells effectively reverses HIV-1 latency. To test if the decreased proviral activation could
153 be explained by GSK484 preventing T cell activation, we determined the abundance of the surface
154 markers CD69 (early activation) and CD25 (late activation). CD25 was not affected by PADI4 inhibition,
155 but for CD69 showed a slight increase after GSK484 exposure (Fig 2E,F). This modest increase in T cell
156 activation is unlikely to explain the reduced HIV-1 transcription, as T cell activation stimulates HIV-1
157 latency reversal. The GSK484 effect on cell proliferation was measured by Ki-67 expression, which
158 remained unaffected by PADI4 inhibition (Fig 2G).
159 To confirm a more general role of PADI4 in HIV-1 latency reversal, we inhibited PADI4 by GSK484 in a
160 K562-derived HIV-1 latency model [34]. In K562-lat cells, the PADI4 gene was expressed (48 copies/10 ng
161 RNA), although at a lower level than in 5A8 of (1800 copies/10 ng) (Fig 2A). This K562-lat cell line is
162 polyclonal with respect to HIV-1 integration sites. As observed for the 5A8 cell line, PADI4 inhibition

163 resulted in reduced PMAi-induced HIV-1 activation (Fig 2H). Inhibiting PADI2 with CAY10723 had no
164 effect alone and no additive effect was observed when inhibiting both PADI2 and PADI4 (Fig 2I),
165 suggesting non-redundancy between the two proteins with respect to HIV-1 latency reversal.
166
167 **Clonal effects of T cell activation and PADI4 inhibition**
168 To test the effect of chronic PADI4 depletion, we attempted to mutate PADI4 by CRISPR. We failed to
169 generate homozygous PADI4-/-mutants and heterozygous mutants expressed wild-type levels of
170 PADI4. However, monoclonal selection revealed that cultures recently derived from a single cell had
171 two different phenotypes with regard to PMAi-induced activation and GSK484 treatment (Fig S2A).
172 Whereas half of the clones responded as the bulk culture to T cell activation (30-40%) and GSK484
173 treatment (23% reduction), half of the clones where easily activated by PMAi (60-80%) and showed a
174 smaller (9%) non-significant effect of GSK484 treatment. Continuous propagation of the cultures
175 reduced this effect. Moreover, the abundance of CD69 marker on the cell surface was significantly
176 increased after GSK484, although not comparable to the CD69 levels after T cell activation (Fig S2B).
177 The clones are expected to be genotypically identical, but as we have showed previously, the provirus
178 in 5A8 bulk culture is epigenetically heterogeneous [35]. The bimodal phenotype could possibly be
179 explained by the chromatin contexts, where the easily activated proviruses are unaffected by PADI4,
180 whereas PADI4 and H3cit play a role in chromatin contexts that have an intermediate latency reversal
181 potential.
182
183 **Effects of prolonged PADI4 depletion**
184 The K562-derived cell model expresses dCas9-KRAB, making it amendable for CRISPRi. We targeted
185 PADI4 with three gene-specific guide RNAs in addition to a non-targeting control. Interestingly, the
186 main effect of this permanent PADI4 reduction was an increase in spontaneous HIV reactivation (Fig
187 S3). The effect of PADI4-depletion did not result in a reduced HIV-1 activation. However, in PADI4-
188 depleted cells, GSK484 had no effect. Rescuing the PADI4-expression by overexpression of PADI4
189 reestablished the parental phenotype. These observations suggests that prolonged PADI4 depletion
190 result in compensatory effects by other mechanisms.
191
192 **Citrullinated histone H3 at the HIV-1 provirus stimulated latency reversal**
193 We next sought to determine the effect of PADI4-inhibition on chromatin during latency reversal. ChIP
194 using antibodies against H3 and H3cit revealed that T cell activation resulted in an increase of H3cit at
195 the HIV-1 promoter (Fig 3A) and that PADI4 inhibition caused an increase in H3 at the HIV-1 promoter
196 (Fig 3B). In the light of previous research [17,18], this was expected. This led us to compare the effect of

197 PADI4 on the HIV-1 promoter using a dedicated chromatin accessibility assay. In addition to more
198 nucleosomes revealed by ChIP, the chromatin at the HIV-1 promoter became more compact after
199 addition of GSK484 alone (Fig 3C). We next compared these results with results from the PLA-ZFP assay
200 where the proviral promoter is marked with an engineered zinc-finger protein (ZFP) that specifically
201 recognizes the HIV-1 LTR [35,36]. This HIV-1 specific ZFP was introduced into 5A8 cells, to generate the
202 1C10 cells, with the proviral promoter marked by the protein. As observed using ChIP, the level of H3cit
203 at the HIV-1 promoter was elevated after T cell stimulation (Fig 3D). This effect was less pronounced
204 in the presence of GSK484, confirming a role for *de novo* PADI4-mediated citrullination at the HIV-1
205 locus during HIV-1 latency reversal. Total histone H3 at the HIV-1 promoter was slightly increased after
206 cell activation (Fig 3E). As expected from previous flow cytometry measurement, GSK484 reduced the
207 GFP signal as observed microscopically (Fig S4A). This technique allows simultaneous detection of H3cit
208 and the effect on HIV-1 activation in single cells. However, due to technical variance, we could not
209 correlate the HIV-1 latency reversal with H3cit levels in individual cells (Fig S4B).
210 We measured the influence of citrullination at three different H3 arginine residues–H3R2, H3R8 and
211 H3R17. Relative to H3, only H3cit8 and H3cit17 increased significantly, with the strongest relative
212 effect on H3cit8 (Fig 3F).
213 To map the distribution of H3cit at the provirus in 5A8 cells, we applied CUT&Tag [37]. Mapping was done
214 using four different conditions, unstimulated or PMAi stimulated cells with or without GSK484 for 24
215 h. In unstimulated cells, two peaks of H3cit were found at the HIV-1 LTR promoter, coinciding with two
216 well-described nucleosomes (nuc-0 and nuc-1) surrounding the transcription start site (Fig 3G). Upon
217 stimulation, the nuc-1 H3cit signal disappeared. Exposure to GSK484 resulted in weaker signals and
218 less clear nucleosome positioning. PMAi induced activation is known to shift or evict nuc-1 of the HIV-
219 1 promoter [38]. Inhibition of PADI4-mediated citrullination has previously been associated with
220 nucleosome repositioning [18].
221
222 **Genome-wide H3cit is stably found at most promoters**
223 The CUT&Tag data provided us with a genome-wide distribution of H3cit in 5A8 cells. Peak calling using
224 MACS2 identified mostly narrow H3cit peaks with a median of 749±20 bp (Fig 4A). Mapping revealed
225 that most (55.4%) H3cit was found at or close to genes (Fig 4B). Aligning the peaks to the transcription
226 start sites of all genes showed that H3cit was predominantly found at promoters, and some in the early
227 coding region (Fig 4C). This global H3cit pattern appears to be stable, as this pattern was not affected
228 by cell stimulation by PMAi or PADI4 inhibition by GSK484 (Fig S5).
229 To relate the H3cit pattern to the distribution of other chromatin marks, we performed a ChromHMM
230 analysis [39]. As expected, the genome-wide H3cit distribution clustered together with histone marks

231 found at open regions of the genome, such as H3K4me3, H3K27ac and H3K4me1 that are found either
232 at promoters or enhancers. The H3cit pattern matched most closely with that of H3K4me3 (Fig 4D).
233 Both H3cit and H3K4me3 are stable marks, associated with open regions, but not necessarily active
234 gene expression [40,41]. On the other hand, marks of heterochromatin such as H3K9me3 and H3K27me3
235 were clustered away from H3cit, as well as H3K36me3, a mark internal to genes where transcription
236 initiation is blocked [42].
237
238 **Productive HIV-1 integrates in H3cit chromatin**
239 Next, we sought to determine the role of H3cit in initial integration of the HIV-1 sequence. We
240 compared the genome-wide map of H3cit to previous integration site data, stratified on the fate of the
241 provirus [43]. As expected from H3cit being found in permissive regions of decondensed chromatin, HIV-
242 1 was enriched in regions with H3cit (Fig 4E). Interestingly, H3cit was most often found at integration
243 sites of productive proviruses. Less H3cit was found at latent or latent reactivatable proviruses,
244 implying that the H3cit structure is resistant to silencing, as previously suggested for HERVs [16].
245
246 **H3cit takes part in activity of T cell receptors genes**
247 No gene set terms were significantly enriched in within the genes associated with H3cit. However, we
248 found 80 genes where new H3cit is formed after PMAi, and 145 genes where the activation-induced
249 citrullination is blocked by GSK484. The overlap was significant as 61 genes were found in both lists
250 (Fisher's exact test, $p<10^{-15}$). Two clusters of gene sets were significantly enriched here: 1) "T-cell
251 receptor", "adaptive immunity", and 2) "citrullination" and "nucleosomes". Upon closer inspection of
252 these, we noted that for a gene set regulated by T cell activation ("GSE13738 Resting vs TCR activated
253 CD4 T cell" [44]), GSK484 led to equally distributed H3cit nucleosomes surrounding the TSS. After
254 activation, few changes were observed (Fig 4F). This observation is consistent with the previously
255 observed redistribution of nucleosomes following PADI4-inhibition by GSK484 treatment [18]. However
256 the PADI4 target seems not to be citrullination of the three H3 residues interrogated here as they
257 remain present.
258 The TNFα promoter is known to be citrullinated after cell stimulation [16]. In agreement, we observed
259 *de novo* H3cit at the TNFα TSS after cell stimulation. This effect was completely abolished in the
260 presence of GSK484 (Fig 4G). This demonstrates the possibility of several roles of H3cit in chromatin
261 during T cell activation.
262
263 ***De novo* H3cit has a general effect on HIV-1 transcription, but not through Tat or acetylation**

264 To test if the effect on the observed loss of GFP in GSK484 treated cells was a result of reduced
265 transcription or a subsequent process, we extracted RNA from the PMAi induced 5A8 cells. HIV-1
266 produces both spliced and unspliced transcripts as to create infectious viruses [13]. We tested the effect
267 of GSK484 on short initiated (5´-LTR), early elongated unspliced (Gag), multiply spliced (Tat-Rev), and
268 late elongated (GFP) transcripts. These transcript types were equally reduced by 30% after GSK484
269 treatment, although significance was only reached for GFP and Tat-Rev (Fig 5A).
270 We next tested if H3cit impaired Tat function. We used PLA-ZFP to detect recruitment of Tat to the LTR
271 in 1C10 cells. Tat was still recruited to the LTR after GSK484 exposure (Fig 5B). Normally Tat is
272 responsible for augmenting the transcription. However, in single cells, the amplitude of GFP expression
273 was not affected by GSK484, only the amount of GFP+ cells, further suggesting no link between Tat
274 and PADI4. To confirm the independence of Tat, we compared J-lat cells with partial HIV-1 genomes,
275 either LTR-GFP (A72), or LTR-Tat-GFP (A2) [31,45]. Both cell lines were exposed to PADI-inhibitors during
276 PMAi stimulation and showed similar levels of GFP reduction after both Cl-amidine and GSK484 (Fig
277 5C). This is consistent with a Tat-independent mechanism.
278 To further explore which host mechanisms are involved in PADI4-mediated HIV-1 transcription, we
279 tested the effect of GSK484 with different latency reversal agents. In addition to PMAi, latency reversal
280 by the protein kinase C agonist Prostratin was affected by GSK484. Latency reversal by HDAC inhibitors
281 Romidepsin and Panabinostat was not affected by GSK484 (Fig 5D). This suggests that the observed
282 effect of PADI4 is either independent from histone acetylation, or that the subset of cells in which
283 PADI4 plays a role for HIV-1 transcription does not overlap with the one activated by HDACi.
284
285 **Heterochromatin forms over the HIV-1 provirus in the absence of H3cit**
286 Given our finding that *de novo* citrullination of H3 and possibly other targets appears to prevent HIV-1
287 transcription in primary cells from PLWH as well as in several model systems, together with the
288 previous finding of H3cit preventing heterochromatin over HERVs [16], we set out to study the impact of
289 H3cit on heterochromatin formation over the HIV-1 provirus. The 5A8 cells have the provirus
290 integrated in a permissive region, and the proviral chromatin is predominantly associated with active
291 histone marks [35]. This chromatin structure mirrors the majority of proviral integration events, as HIV-
292 1 tends to target open chromatin [46]. However, once ART is initiated, new infections are prevented. The
293 immune system targets cells producing viral proteins, resulting in an advantage of latently infected
294 cells. Long-term ART results in the provirus being found in epigenetically silent regions [6]. To replicate
295 this epigenetic state, we modified the 5A8 cells to silence the provirus. We tethered a KRAB (Krüppel
296 Associated Box) domain to the engineered ZFP that specifically recognizes the HIV-1 provirus used for
297 the PLA experiments [35]. We introduced this KRAB-ZFP protein into the cells and selected for
298 monoclonal cell lines. We characterized two clones in particular, 2C10 with the ZFP-KRAB, and 1C10–

299 the control cell line with only the ZFP construct. In the 2C10 cells, H3K9me3 at the promoter was
300 confirmed by ChIP (Fig 6A). The HIV-1 inducibility after 24 h PMAi stimulation was lower in 2C10
301 compared to the control 5A8 clone 1C10 (Fig 6B). Among the cells that still had inducible HIV-1, GSK484
302 further reduced the reactivation. As expected from less HIV-1 reactivation, the recruitment of Tat was
303 less significant in the 2C10 cells (Fig 6C). This shows a limited effect of H3cit in established
304 heterochromatin.
305 Next we wanted to investigate if H3cit prevents heterochromatin development. We hypothesized that
306 *de novo* citrullination of the HIV-1 promoter prevents HP1α binding and functional heterochromatin
307 formation, despite occurrence of H3K9me3. From a previous study [35], we know that following
308 activation H3K9me3 levels increase at the HIV-1 provirus. We confirmed this finding using ChIP (Fig
309 6D). However, H3K9me3 is not sufficient to establish heterochromatin. To form functional
310 heterochromatin, the H3K9me3 should be enclosed in HP1α. In HERVs, H3cit8 hinders HP1α binding
311 to H3K9me3 [16]. Consequently, by activating the cells and preventing citrullination by GSK484, HP1α
312 would be given a platform to bind. We tested the recruitment of HP1α to the HIV-1 promoter by both
313 ChIP (Fig 6D) and PLA (Fig 6E). Consistently using both techniques, HP1α binds specifically to HIV-1
314 after cell stimulation when PADI4 is inhibited. In the 2C10 cells, where the provirus was embedded in
315 heterochromatin before the T cell stimulation, HP1α was not found above background levels (Fig 6E).
316
317 **H3cit partly inhibited HUSH-mediated chromatin silencing**
318 New heterochromatin formation over foreign DNA can be directed by the HUSH complex [47]. To test if
319 our observations can be explained by HUSH, we reduced expression of HUSH component TASOR by
320 shRNA, as well as ectopically expressed VPX that is known to repress HUSH [48]. In 5A8 cells, the latency
321 reversal effect of GSK484 after T cell activation depended significant on HUSH (Fig6F). However, only
322 part of the effect (approx. 20%) could be explained by HUSH.
323

324 ## Discussion

325 In this study, we demonstrated that *de novo* PADI4-mediated citrullination of histone H3 at the HIV-1
326 promoter inhibits the formation of heterochromatin and promotes HIV-1 transcription following cell
327 activation. When PADI4 activity was blocked during cell activation, new citrullination of proviral
328 nucleosomes did not occur, allowing stable heterochromatin to form. The HUSH complex was partly
329 involved in the heterochromatin formation, but the main effect appeared to come from an
330 unidentified source. Proviruses within citrullinated chromatin were resistant to epigenetic silencing.
331 This mechanism is particularly relevant for HIV-1 proviruses integrated in permissive chromatin
332 regions, which are less prone to latency and more responsive to latency reversal agents. Inhibiting *de*

333 *novo* H3cit induces chromatin compaction at the HIV-1 promoter. We also provide the first genome-
334 wide map of H3 citrullination in T cells, showing that this mark is enriched at promoters and associated
335 with permissive chromatin.
336
337 **Implications for the reservoir in people living with HIV-1**
338 We have uncovered a mechanism that explains one aspect of the differences in the HIV-1 reservoir
339 between chronic viremia and after long term ART in PWH. Cells continuously producing viruses
340 undergo cytopathic effects and are targeted by the immune system [7,49]. We observe a mechanism that
341 is active in viremic individuals but contributes less after long term ART. The latent reservoir is, at least
342 in part, transcriptionally active [1,3,28,50]. Our study highlights the heterogeneity of the reservoir,
343 particularly during chronic infection before ART. When ART is initiated, pressure to induce
344 reactivatable latent proviruses increases. The intact viruses date to the time of ART initiation [51]. The
345 state of the reservoir when ART is initiated is key for post-treatment control and a potential HIV-1 cure
346 [52]. Over time an increasing fraction of the intact provirus is found in heterochromatin [6]. Part of the
347 reservoir is susceptible to histone acetylation and can be cleared even under ART [53]. Future studies are
348 required to reveal the fate of the cells with citrullination at the promoter, that cannot be epigenetically
349 silenced after ART initiation. Many of these cells are likely eliminated through cytopathic effects or
350 immune detection, unless they are cytotoxic CD4 T cells which resist cell death[50]. A subset of proviruses
351 might become latent solely as a consequence of the cell entering a resting state [54], and then stochastic
352 events cause reactivation [55]. This points to the possibility of reducing the fraction of the reservoir that
353 is subject to stochastic reactivation by manipulating PADI4 during initiation of ART.
354
355 **Epigenetic interplay of H3cit and other PADI4 targets**
356 H3cit is linked to active transcription and open chromatin across various cellular contexts [16,25–27]. In
357 addition to H3, PADI4 targets numerous proteins in the nucleus, including histone H1 and HP1γ [25,27].
358 We cannot exclude that modifications of these proteins also play a role in the phenotype we observe.
359 Here we detailed the role of H3cit8. Notably, other H3 residues can also be citrullinated, potentially
360 influencing the cell differently. The H3cit26 mark is recognized by SMARCD1, that has been suggested
361 as a link between H3cit and heterochromatin [26]. In mice ES cells, H3cit26 and H3K9me3 do not
362 colocalize at basal levels. However, after PADI inhibition, H3K9me3 levels appear at the sites of H3cit26
363 [26]. Arginines, which can be citrullinated, are often found adjacent to lysines, key residues for epigenetic
364 modifications. Moreover, arginine methylation and citrullination are mutually exclusive [20]. Both
365 arginine methylation and citrullination are stable histone modifications and whereas a short pulse of
366 PADI4 inhibition is unlikely to shift the balance between methylated and citrullinated arginine residues,
367 prolonged reduced levels of PADI4 could have this effect [18]. Arginine methylation of H3 through CARM1

368 has a known repressive effect on HIV-1 latency [56]. We conclude that PADI4 plays a balancing role in
369 HIV-1 transcription, depending on both the cell type and the site of proviral integration.
370
371 **Limitations of the study**
372 Our study is confined to CD4 T cells from peripheral blood, despite the presence of the HIV-1 reservoir
373 at several other anatomical sites in the body. While our findings are grounded in clinical samples, the
374 mechanistic insights primarily derive from cell models. We were unable to track PADI4-depleted cells
375 as they reverted to latency to determine if they were prevented from subsequent reactivation. To
376 enhance the generalizability and applicability of the findings, we employed several different cell
377 models and complementary techniques. However, we were unable to test our hypothesis *in vivo* or in
378 animal models. The small sample size in parts of the test is a limitation for the generalizability.
379
380 **Conclusions**
381 Our findings reveal a novel epigenetic mechanism that regulates HIV-1 transcription and latency,
382 suggesting that PADI4 could serve as a potential therapeutic target for interventions aimed at reducing
383 the size of the latent reservoir required for a future HIV-1 cure.
384

385 ## Methods

386 **Cell Culture and isolation**
387 J-lat 5A8, 1C10, K562 and all primary cells were cultured in cytokine-free media (RPMI 1640 medium
388 (Hyclone, Cat# SH30096_01), 10% FBS (Life Technologies, Cat# 10270–106), 1% Glutamax (Life
389 Technologies, Cat# 35050), 1% Penicillin-streptomycin (Life Technologies, Cat# 15140–122)).
390 Primary cells were obtained from 50 ml of fresh blood from study participants (Ethical permits
391 2017/1138-31/4 and 2018/102-31/1). Blood samples were diluted with an equal amount of PBS and
392 carefully overlayed on Ficoll-Paque Plus solution (Cytiva, Cat# 17144003). Centrifugation was
393 conducted at RT and 400 g for 30 minutes without brake. Resting CD4 T cells were isolated from the
394 obtained PBMCs by a two-step magnetic isolation using the Miltenyi Biotec magnetic associated cell
395 sorting (MACS) platform. For the first step, the CD4 negative cell isolation kit (Cat# 130-096-533) was
396 used according to the manufacturer's protocol. Secondly, resting CD4 T cells were negatively selected
397 with magnetic beads against the activation markers CD25, CD69 and HLA-DR.
398
399 **Cell activation**
400 CD4 T cells isolated from peripheral blood and immediately put in *ex vivo* culture. After 16 h resting,
401 cells were exposed to PADI4 inhibitor GSK484 for 3 h followed by T cell activation by phorbol-12-
402 myristate-13-acetate and ionomycin (PMAi) for 21 h. Both DNA and RNA were extracted from the cells,

403 and culture supernatant RNA was extracted to quantitate release of viral particles. DNA was extracted
404 either by Allprep (Qiagen, Cat#80204) or QIAamp DNA Mini Kit (Qiagen, Cat#51304). Viral RNA was
405 isolated by QIAamp Viral RNA Mini Kit (Qiagen, Cat#52904). The DNA was used to measure the HIV-1
406 reservoir using IPDA [29]. For cell associated RNA, the LTR region and the multiply spliced RNA was
407 investigated separately. Cell-free RNA was measured by the amount of intact virus RNA in the
408 supernatant [30].
409
410 **Chemicals to induce proviral activation**
411 Cells were exposed to latency reversal agents as indicated with the following concentrations used:
412 Phorbol 12-myristate 13-acetate (PMA, Sigma-Aldrich Cat# 79346) final concentration 50 ng/ml,
413 ionomycin (Sigma-Aldrich Cat# I0634) final concentration 1 µM. Ingenol-3-angelate PEP005 (Sigma-
414 Aldrich, Cat# SML1318) final concentration 12 nM, panobinostat (Cayman Chemicals, Cat#
415 CAYM13280) final concentration or 150 nM, JQ1 (Cayman Chemicals, Cat#CAYM11187) final
416 concentration 100 nM, prostratin (Sigma-Aldrich, Cat#P0077) final concentration 6 µM.
417 PADI4 inhibitor GSK484 (MCE HY-100514) was added, if applicable, at a final concentration of 10 µM.
418 Pan PADI inhibitor Cl-Amidine (Cayman Chemicals. Cat#CAYM10599) was added at a final
419 concentration of 200 µM. Inactive GSK484 and GSK199 control GSK106 (MCE HY-120343) was added
420 at a final concentration of 10 µM. Padi4 Inhibitor GSK199 (MCE HY-103058) was added at a final
421 concentration of 10 µM
422
423 **Flow cytometry**
424 Cells were stained with LIVE/DEAD Fixable Violet Dead Cell Stain (Thermo Scientific, Cat# L34955) and
425 fixed in 2% formaldehyde for 15 min. if required Flow analysis was performed on a CytoFLEX S
426 (Beckman Coulter). Individual flow droplets were gated for lymphocytes, viability, and singlets. Data
427 were analyzed by Flowjo 10.1 (Tree Star).
428 When staining for CD25 and CD69. Cells were washed with PBS (Gibco #18912014) + 0.5% BSA (FACS
429 buffer) then incubated with 1/100 CD25 (BD, Cat#555434) and CD69 1/20 (BD, Cat# 560711) antibody
430 diluted in FACS Buffer for 30 min at 4°C. Cells were then washed with 100ul of FACS buffer then
431 resuspended in 100ul FACS buffer and 1/1000 dilution of Live/dead stain (Thermo Scientific, Cat#
432 L34964) and incubated for 15 min at 4°C. Cells were washed in 100 µl FACS buffer then resuspended
433 in 2% formaldehyde PBS for 15 min in the dark at room temperature. Finally, cells were resuspended
434 in 100 µl of ice-cold PBS prior to flow cytometry.
435 When staining for KI-67 cells were washed twice with PBS and resuspended by vortexing while adding
436 ice cold 70% Ethanol. This was followed by a 1 h incubation at -20°C, three washed with FACS buffer
437 then resuspension in FACS buffer at $1x10^6$ cells/ml. 5 µl of APC anti-human Ki-67 Antibody (BioLegend,

438 CAT# 350513) in 100 µL of cell solution. This was incubated for 30 min in the dark at room temperature,
439 washed with FACS buffer then resuspended in 100 µl of ice-cold PBS prior to flow cytometry.
440
441 **KRAB domain expression in 5A8 cells**
442 The KRAB domain from pHR-SFFV-dCas9-BFP-KRAB (Addgene plasmid #46911) was cloned into plasmid
443 pHR-SFFV-ZF3-P2A-BFP using Gibson assembly (New England Biolabs Cat#E2611S) by substituting the
444 KRAB region in between the ZFP3 and P2A region.
445 The contruct was co-transfected with psPAX and pMD2.G into HEK293T cells using lipofectamine LTX
446 (Invitrogen Cat# 15338030) according to the manufacturer's instructions. 20 µL of the viral supernatant
447 was added to 180 µL of K562-Lat cell culture in a round bottom 96 well plate and spinoculated for 300g
448 for 1hr at room temperature. These were puromycin selected with 1.5 µg/ml puromycin RPMI media
449 for 5 days.
450
451 **Immunoblotting**
452 Cell pellets were lysed in lysis buffer (150 mM NaCl, 50 mM Tris, 1% Triton-X100, 1 mM orthovanadate).
453 Protein concentrations were calculated using Bradford assay (Bio-Rad Cat#5000006). Human Histone
454 H3 (citrulline R2 + R8 + R17) peptide (Abcam, Cat# ab32876) was used in a competition assay. Samples
455 were diluted to 1× Laemmli buffer (Bio-Rad, Cat# 1610747) with 10 mM DTT. Samples were heated for
456 10 min at 70°C and then loaded on a 12% Mini-protean TGX gel (Bio-Rad Cat# 4561044). The gels were
457 run for approximately 1 h at 100 V. Proteins were transferred onto a PVDF membrane (Bio-Rad, Cat#
458 1704156) and blocked in 5% skimmed milk in PBS-T for 1 h at room temperature. Afterwards, the
459 membrane was incubated at 4°C overnight with primary antibodies (1:1000) in 1% milk in PBS-T. We
460 used primary antibodies as above. After washing and addition of secondary HRP-conjugated
461 antibodies, membranes were developed using Pierce ECL Plus Western Blotting Substrate (Thermo
462 Scientific Cat# 32132). Membranes were stripped (Restore plus Western blot stripping buffer Thermo
463 Scientific Cat# 46430) and re-probed using a second set of control primary antibodies. Blots were run
464 and visualized using iBright FL1500 Imaging System (ThermoFisher).
465
466 **Chromatin immunoprecipitation**
467 ChIP-qPCR was performed using the iDeal ChIP-qPCR protocol (Diagenode, Cat# C01010180). Each ChIP
468 reaction was performed on 2×10^6 cells. Cells were fixed with 11% formaldehyde for 10 min in room
469 temperature. Sonication was performed at 30 s in eight cycles (Bioruptor Pico, Diagenode, Cat#
470 B01060010). ChIP was performed using antibody. ChIP eluates were purified with Wizard SV Gel and
471 PCR clean-up system (Promega, Cat# A9282). Primer sequences are shown in Table S2. PCR reactions

472 were performed with Powerup SYBR green master mix (2×) (ThermoFisher, Cat#A25742) using 40
473 cycles on an Applied Biosystems 7500 Fast Real-Time PCR System (ThermoFisher).
474
475 **CUT&Tag seq**
476 Version 3 CUT&Tag protocol (Kaya-Okur and Henikoff, 2020) was used as described. A 1/400 dilution
477 of Anti-Histone H3 (citrulline R2 + R8 + R17) antibody (Abcam, Cat# ab5103) was used per sample.
478 Thirteen cycles of PCR were used for amplifying the libraries. Reads were trimmed, then, mapped onto
479 the GB38 human reference genome with Bowtie2.
480
481 **Gene set enrichment**
482 Genes with log2 ratio>0.5 difference between DMSO and PMAi, or PMAi and PMAi, GSK484 were
483 selected (Table S3). The lists were analyzed using the DAVID tool [57].
484
485 **Proximity ligation assay (PLA)**
486 Cells were adhered to coated polylysine coated microscope slides (VWR, Cat#6310107) marked with a
487 hydrophobic barrier using A-PAP pen (Histolab, Cat# 08046N) and a modified PLA protocol was
488 followed. In short, cells were washed with PBS and allowed to settle onto the polylysine slides). PLA
489 was performed according to the manufacturer's protocol (Sigma-Aldrich, cat#Duo92007) with a few
490 modifications: PLA plus and minus probes were diluted 1:20, amplification buffer (5×) was used at 10×.
491 All washes were performed in PBS. Antibodies (1:1,000) were used against Tat (Abcam Cat#43014),
492 FLAG M2 (Sigma-Aldrich Cat# F1804 lot SLCF4933), H3 (Abcam, Cat# ab1791), H3R2cit (Abcam, Cat#
493 ab176843), H3R8cit (Abcam, Cat# ab219406), H3R17cit (Abcam, Cat# ab219407),
494 H3R2cit+R8cit+R17cit (Abcam Cat# ab5103). Before DAPI staining (Life technologies, Cat# 62248) and
495 mounted with mounting medium with DAPI (Sigma-Aldrich, Cat# DUO82040), FITC-conjugated anti-
496 GFP (Abcam, Cat#ab6662) was applied (1:1000) for 1 hour at ambient temperature protected from
497 light. Coverslips (VWR, Cat# MARI0117530) were sealed onto slide with nail polish and stored at 4°C
498 overnight before imaging. Slides were imaged using a Panoramic Midi II slide scanner (3DHistech) and
499 images were exported using the CaseViewer application. Images were analyzed with ImageJ (version
500 2.0.0-rc-69/1.52) and macros developed in house. Each RGB image was separated into separate
501 channels. Based on the blue (DAPI) channel, nuclei were identified. In the red channel, spots
502 ("maxima") were detected with thresholds 6–48.
503
504 **Quantitative PCR (qPCR)**
505 RNA was extracted from cells using RNeasy plus kit (Qiagen Cat#74134) according to the manufacturers
506 instructions. Then cDNA was made using Revertaid as described (Thermo Scientific Cat#K1621). The

507 cDNA was diluted 1/10 in distilled water and used with 400 nM of each primer (final concentration)
508 and SYBR Green Master Mix for qPCR (Fisher Scientific Cat# A25742) in a Microamp Fast Optical 96
509 Well Reaction Plate (Fisher Scientific Cat#4346906). The PCRs were run using Applied Biosystems 7500
510 Fast Real-Time PCR System with 40 cycles.
511
512 **Digital droplet PCR (ddPCR)**
513 ddPCR was performed with the QX200 Droplet Digital qPCR System (Bio-Rad). Each reaction consisted
514 of 20 µL, containing 10 µL Supermix for Probes without dUTP (Bio-Rad, Cat# 1863024), 900 nM primers,
515 250 nM probe (labelled with HEX or FAM), and 8 µL undiluted cellular DNA. RT-ddPCR was used
516 according to [30], using 11 µL undiluted RNA and the One-Step RT-ddPCR Advanced Kit for Probes (Bio-
517 Rad, Cat# 1864021). Droplets were generated. Emulsified PCR reactions were performed with a C1000
518 Touch thermal cycler (Bio-Rad), with the following protocol: 95°C for 10 min, followed by 40 cycles of
519 94°C for 30 s and 57°C for 60 s, and a final droplet cure step of 10 min at 98°C. Each well was then read
520 with a QX200 Droplet Reader (Bio-Rad). Droplets were analysed with QuantaSoft version 1.5 (Bio-Rad)
521 software in the absolute quantification mode.
522
523 **Data availability**
524 The datasets generated in this study is publicly available through the Gene Expression Omnibus (GEO)
525 GSE273899
526

527 ## Acknowledgements

528 We are most grateful to the study participants without whom this study would not have been possible.
529 We would also like to thank BEA, MedH flow facility, as well as Mukesh Varshney and Zhichang Huang
530 for technical assistance. Funding: This study was supported by grants from CIMED FoUI-973749, VR
531 2019–00991, KI 2019-00846, Cancerfonden 190412Pj (to J.P.S.), Swedish Physicians Against AIDS
532 Research Foundation FOb2020-0004 (to J.P.S), FOa2022-0001, FOa2023-0003 (to B.B.J.), KI Foundation
533 for Virus Research 2024-00634 (to L.L.).

534 ## Author contributions

535 Conceptualization, L.L., J.P.S.; investigation and validation, L.L, B.B.J., B.L., H.R., J.P.S.; clinical
536 recruitment, P.N., O.K.; supervision, J.P.S.; funding acquisition, J.P.S. and B.B.J. Writing – original draft,
537 L.L., B.B.J., and J.P.S.; review & editing, all co-authors.

538 ## Declaration of interests

539 The authors declare no competing interests.

540

541 ## References

542 1. Yukl, S.A., Kaiser, P., Kim, P., Telwatte, S., Joshi, S.K., Vu, M., Lampiris, H., and Wong, J.K. (2018).
543 HIV latency in isolated patient CD4(+) T cells may be due to blocks in HIV transcriptional
544 elongation, completion, and splicing. Sci. Transl. Med. *10*. https://doi.org/ARTN eaap9927
545 10.1126/scitranslmed.aap9927.

546 2. Moron-Lopez, S., Kim, P., Sogaard, O.S., Tolstrup, M., Wong, J.K., and Yukl, S.A. (2019).
547 Characterization of the HIV-1 transcription profile after romidepsin administration in ART-
548 suppressed individuals. Aids *33*, 425–431. https://doi.org/10.1097/QAD.0000000000002083.

549 3. Dubé, M., Tastet, O., Dufour, C., Sannier, G., Brassard, N., Delgado, G.-G., Pagliuzza, A., Richard,
550 C., Nayrac, M., Routy, J.-P., et al. (2023). Spontaneous HIV expression during suppressive ART is
551 associated with the magnitude and function of HIV-specific CD4+ and CD8+ T cells. Cell Host
552 Microbe *31*, 1507-1522.e5. https://doi.org/10.1016/j.chom.2023.08.006.

553 4. Einkauf, K.B., Lee, G.Q., Gao, C., Sharaf, R., Sun, X., Hua, S., Chen, S.M., Jiang, C., Lian, X.,
554 Chowdhury, F.Z., et al. (2019). Intact HIV-1 proviruses accumulate at distinct chromosomal
555 positions during prolonged antiretroviral therapy. J. Clin. Invest. *129*, 988–998.
556 https://doi.org/10.1172/JCI124291.

557 5. Jiang, C., Lian, X., Gao, C., Sun, X., Einkauf, K.B., Chevalier, J.M., Chen, S.M.Y., Hua, S., Rhee, B.,
558 Chang, K., et al. (2020). Distinct viral reservoirs in individuals with spontaneous control of HIV-1.
559 Nature *585*, 261–267. https://doi.org/10.1038/s41586-020-2651-8.

560 6. Lian, X., Seiger, K.W., Parsons, E.M., Gao, C., Sun, W., Gladkov, G.T., Roseto, I.C., Einkauf, K.B.,
561 Osborn, M.R., Chevalier, J.M., et al. (2023). Progressive transformation of the HIV-1 reservoir cell
562 profile over two decades of antiviral therapy. Cell Host Microbe *31*, 83-96.e5.
563 https://doi.org/10.1016/j.chom.2022.12.002.

564 7. Simonetti, F.R., Zhang, H., Soroosh, G.P., Duan, J., Rhodehouse, K., Hill, A.L., Beg, S.A.,
565 McCormick, K., Raymond, H.E., Nobles, C.L., et al. (2020). Antigen-driven clonal selection shapes
566 the persistence of HIV-1 infected CD4+ T cells in vivo. J. Clin. Invest.
567 https://doi.org/10.1172/jci145254.

568 8. Jütte, B.B., Love, L., and Svensson, J.P. (2023). Molecular Mechanisms of HIV-1 Latency from a
569 Chromatin and Epigenetic Perspective. Curr. Clin. Microbiol. Rep. *10*, 246–254.
570 https://doi.org/10.1007/s40588-023-00208-3.

571 9. Tchasovnikarova, I.A., Timms, R.T., Matheson, N.J., Wals, K., Antrobus, R., Göttgens, B., Dougan,
572 G., Dawson, M.A., and Lehner, P.J. (2015). Epigenetic silencing by the HUSH complex mediates
573 position-effect variegation in human cells. Science *348*, 1481.
574 https://doi.org/10.1126/science.aaa7227.

575 10. du Chéné, I., Basyuk, E., Lin, Y.-L., Triboulet, R., Knezevich, A., Chable-Bessia, C., Mettling, C.,
576 Baillat, V., Reynes, J., Corbeau, P., et al. (2007). Suv39H1 and HP1gamma are responsible for
577 chromatin-mediated HIV-1 transcriptional silencing and post-integration latency. EMBO J. *26*,
578 424–435. https://doi.org/10.1038/sj.emboj.7601517.

579 11. Mateescu, B., Bourachot, B., Rachez, C., Ogryzko, V., and Muchardt, C. (2008). Regulation of an
580 inducible promoter by an HP1beta-HP1gamma switch. EMBO Rep. *9*, 267–272.
581 https://doi.org/10.1038/embor.2008.1.

582 12. Marban, C., Suzanne, S., Dequiedt, F., de Walque, S., Redel, L., Van Lint, C., Aunis, D., and Rohr,
583 O. (2007). Recruitment of chromatin-modifying enzymes by CTIP2 promotes HIV-1
584 transcriptional silencing. EMBO J. *26*, 412–423. https://doi.org/10.1038/sj.emboj.7601516.

585 13. Purcell, D.F., and Martin, M.A. (1993). Alternative splicing of human immunodeficiency virus type
586 1 mRNA modulates viral protein expression, replication, and infectivity. J. Virol. *67*, 6365–6378.
587 https://doi.org/10.1128/JVI.67.11.6365-6378.1993.

588 14. Berro, R., Kehn, K., de la Fuente, C., Pumfery, A., Adair, R., Wade, J., Colberg-Poley, A.M., Hiscott,
589 J., and Kashanchi, F. (2006). Acetylated Tat regulates human immunodeficiency virus type 1
590 splicing through its interaction with the splicing regulator p32. J. Virol. *80*, 3189–3204.
591 https://doi.org/10.1128/JVI.80.7.3189-3204.2006.

592 15. Seczynska, M., Bloor, S., Cuesta, S.M., and Lehner, P.J. (2022). Genome surveillance by HUSH-
593 mediated silencing of intronless mobile elements. Nature *601*, 440–445.
594 https://doi.org/10.1038/s41586-021-04228-1.

595 16. Sharma, P., Azebi, S., England, P., Christensen, T., Møller-Larsen, A., Petersen, T., Batsché, E., and
596 Muchardt, C. (2012). Citrullination of histone H3 interferes with HP1-mediated transcriptional
597 repression. PLoS Genet. *8*, e1002934. https://doi.org/10.1371/journal.pgen.1002934.

598 17. Jentink, N., Purnell, C., Kable, B., Swulius, M.T., and Grigoryev, S.A. (2023). Cryoelectron
599 tomography reveals the multiplex anatomy of condensed native chromatin and its unfolding by
600 histone citrullination. Mol. Cell *83*, 3236-3252.e7. https://doi.org/10.1016/j.molcel.2023.08.017.

601 18. Moshkovich, N., Ochoa, H.J., Tang, B., Yang, H.H., Yang, Y., Huang, J., Lee, M.P., and Wakefield,
602 L.M. (2020). Peptidylarginine Deiminase IV Regulates Breast Cancer Stem Cells via a Novel Tumor
603 Cell-Autonomous Suppressor Role. Cancer Res. *80*, 2125–2137. https://doi.org/10.1158/0008-
604 5472.CAN-19-3018.

605 19. Bannister, A.J., Zegerman, P., Partridge, J.F., Miska, E.A., Thomas, J.O., Allshire, R.C., and
606 Kouzarides, T. (2001). Selective recognition of methylated lysine 9 on histone H3 by the HP1
607 chromo domain. Nature *410*, 120–124. https://doi.org/10.1038/35065138.

608 20. Cuthbert, G.L., Daujat, S., Snowden, A.W., Erdjument-Bromage, H., Hagiwara, T., Yamada, M.,
609 Schneider, R., Gregory, P.D., Tempst, P., Bannister, A.J., et al. (2004). Histone Deimination
610 Antagonizes Arginine Methylation. Cell *118*, 545–553.
611 https://doi.org/10.1016/j.cell.2004.08.020.

612 21. Cherrington, B.D., Morency, E., Struble, A.M., Coonrod, S.A., and Wakshlag, J.J. (2010). Potential
613 Role for Peptidylarginine Deiminase 2 (PAD2) in Citrullination of Canine Mammary Epithelial Cell
614 Histones. PLoS ONE *5*, e11768. https://doi.org/10.1371/journal.pone.0011768.

615 22. Nakashima, K., Hagiwara, T., and Yamada, M. (2002). Nuclear Localization of Peptidylarginine
616 Deiminase V and Histone Deimination in Granulocytes. J. Biol. Chem. *277*, 49562–49568.
617 https://doi.org/10.1074/jbc.M208795200.

618 23. Vossenaar, E.R. (2004). Expression and activity of citrullinating peptidylarginine deiminase
619 enzymes in monocytes and macrophages. Ann. Rheum. Dis. *63*, 373–381.
620 https://doi.org/10.1136/ard.2003.012211.

621 24. Chang, X., Han, J., Pang, L., Zhao, Y., Yang, Y., and Shen, Z. (2009). Increased PADI4 expression in
622 blood and tissues of patients with malignant tumors. BMC Cancer *9*, 40.
623 https://doi.org/10.1186/1471-2407-9-40.

624 25. Christophorou, M.A., Castelo-Branco, G., Halley-Stott, R.P., Oliveira, C.S., Loos, R.,
625 Radzisheuskaya, A., Mowen, K.A., Bertone, P., Silva, J.C.R., Zernicka-Goetz, M., et al. (2014).
626 Citrullination regulates pluripotency and histone H1 binding to chromatin. Nature *507*, 104–108.
627 https://doi.org/10.1038/nature12942.

628 26. Xiao, S., Lu, J., Sridhar, B., Cao, X., Yu, P., Zhao, T., Chen, C.-C., McDee, D., Sloofman, L., Wang, Y.,
629 et al. (2017). SMARCAD1 Contributes to the Regulation of Naive Pluripotency by Interacting with
630 Histone Citrullination. Cell Rep. *18*, 3117–3128. https://doi.org/10.1016/j.celrep.2017.02.070.

631 27. Wiese, M., Bannister, A.J., Basu, S., Boucher, W., Wohlfahrt, K., Christophorou, M.A., Nielsen,
632 M.L., Klenerman, D., Laue, E.D., and Kouzarides, T. (2019). Citrullination of HP1γ chromodomain
633 affects association with chromatin. Epigenetics Chromatin *12*, 21.
634 https://doi.org/10.1186/s13072-019-0265-x.

635 28. Lindqvist, B., Svensson Akusjarvi, S., Sonnerborg, A., Dimitriou, M., and Svensson, J.P. (2020).
636 Chromatin maturation of the HIV-1 provirus in primary resting CD4+ T cells. Plos Pathog. *16*,
637 e1008264. https://doi.org/10.1371/journal.ppat.1008264.

638 29. Bruner, K.M., Wang, Z., Simonetti, F.R., Bender, A.M., Kwon, K.J., Sengupta, S., Fray, E.J., Beg,
639 S.A., Antar, A.A.R., Jenike, K.M., et al. (2019). A quantitative approach for measuring the
640 reservoir of latent HIV-1 proviruses. Nature. https://doi.org/10.1038/s41586-019-0898-8.

641 30. Martin, H.A., Kadiyala, G.N., Telwatte, S., Wedrychowski, A., Chen, T.-H., Moron-Lopez, S.,
642 Arneson, D., Hoh, R., Deeks, S., Wong, J., et al. (2022). New Assay Reveals Vast Excess of
643 Defective over Intact HIV-1 Transcripts in Antiretroviral Therapy-Suppressed Individuals. J. Virol.,
644 e0160522. https://doi.org/10.1128/jvi.01605-22.

645 31. Jordan, A., Bisgrove, D., and Verdin, E. (2003). HIV reproducibly establishes a latent infection
646 after acute infection of T cells in vitro. Embo J. *22*, 1868–1877.

647 32. Sakane, N., Kwon, H.S., Pagans, S., Kaehlcke, K., Mizusawa, Y., Kamada, M., Lassen, K.G., Chan, J.,
648 Greene, W.C., Schnoelzer, M., et al. (2011). Activation of HIV Transcription by the Viral Tat
649 Protein Requires a Demethylation Step Mediated by Lysine-specific Demethylase 1
650 (LSD1/KDM1). Plos Pathog. *7*. https://doi.org/ARTN e1002184 10.1371/journal.ppat.1002184.

651 33. Asaga, H., Nakashima, K., Senshu, T., Ishigami, A., and Yamada, M. (2001). Immunocytochemical
652 localization of peptidylarginine deiminase in human eosinophils and neutrophils. J. Leukoc. Biol.
653 *70*, 46–51.

654 34. Besnard, E., Hakre, S., Kampmann, M., Lim, H.W., Hosmane, N.N., Martin, A., Bassik, M.C.,
655 Verschueren, E., Battivelli, E., Chan, J., et al. (2016). The mTOR Complex Controls HIV Latency.
656 Cell Host Microbe *20*, 785–797. https://doi.org/10.1016/j.chom.2016.11.001.

657 35. Lindqvist, B., Jütte, B.B., Love, L., Assi, W., Roux, J., Sönnerborg, A., Tezil, T., Verdin, E., and
658 Svensson, J.P. (2022). T cell stimulation remodels the latently HIV-1 infected cell population by
659 differential activation of proviral chromatin. PLoS Pathog. *18*, e1010555.
660 https://doi.org/10.1371/journal.ppat.1010555.

661 36. Wang, P., Qu, X., Wang, X., Zhu, X., Zeng, H., Chen, H., and Zhu, H. (2014). Specific reactivation of
662 latent HIV-1 with designer zinc-finger transcription factors targeting the HIV-1 5 ’-LTR promoter.
663 Gene Ther. *21*, 490–495. https://doi.org/10.1038/gt.2014.21.

664 37. Kaya-Okur, H.S., Wu, S.J., Codomo, C.A., Pledger, E.S., Bryson, T.D., Henikoff, J.G., Ahmad, K., and
665 Henikoff, S. (2019). CUT&Tag for efficient epigenomic profiling of small samples and single cells.
666 Nat. Commun. *10*, 1930. https://doi.org/10.1038/s41467-019-09982-5.

667 38. Van Lint, C., Emiliani, S., Ott, M., and Verdin, E. (1996). Transcriptional activation and chromatin
668 remodeling of the HIV-1 promoter in response to histone acetylation. EMBO J. *15*, 1112–1120.

669 39. Ernst, J., and Kellis, M. (2017). Chromatin-state discovery and genome annotation with
670 ChromHMM. Nat. Protoc. *12*, 2478–2492. https://doi.org/10.1038/nprot.2017.124.

671 40. Santos-Rosa, H., Schneider, R., Bannister, A.J., Sherriff, J., Bernstein, B.E., Emre, N.C.T., Schreiber,
672 S.L., Mellor, J., and Kouzarides, T. (2002). Active genes are tri-methylated at K4 of histone H3.
673 Nature *419*, 407–411. https://doi.org/10.1038/nature01080.

674 41. Howe, F.S., Fischl, H., Murray, S.C., and Mellor, J. (2017). Is H3K4me3 instructive for transcription
675 activation? BioEssays *39*, 1–12. https://doi.org/10.1002/bies.201600095.

676 42. Bannister, A.J., Schneider, R., Myers, F.A., Thorne, A.W., Crane-Robinson, C., and Kouzarides, T.
677 (2005). Spatial Distribution of Di- and Tri-methyl Lysine 36 of Histone H3 at Active Genes. J. Biol.
678 Chem. *280*, 17732–17736. https://doi.org/10.1074/jbc.M500796200.

679 43. Battivelli, E., Dahabieh, M.S., Abdel-Mohsen, M., Svensson, J.P., Da Silva, I.T., Cohn, L.B.,
680 Gramatica, A., Deeks, S., Greene, W.C., Pillai, S.K., et al. (2018). Distinct chromatin functional
681 states correlate with HIV latency reactivation in infected primary CD4(+) T cells. Elife *7*.
682 https://doi.org/ARTN e34655 10.7554/eLife.34655.

683 44. Bangs, S.C., Baban, D., Cattan, H.J., Li, C.K.-F., McMichael, A.J., and Xu, X.-N. (2009). Human CD4+
684 Memory T Cells Are Preferential Targets for Bystander Activation and Apoptosis. J. Immunol.
685 *182*, 1962–1971. https://doi.org/10.4049/jimmunol.0802596.

686 45. Jordan, A., Defechereux, P., and Verdin, E. (2001). The site of HIV-1 integration in the human
687 genome determines basal transcriptional activity and response to Tat transactivation. EMBO J.
688 *20*, 1726–1738. https://doi.org/10.1093/emboj/20.7.1726.

689 46. Schröder, A.R.W., Shinn, P., Chen, H., Berry, C., Ecker, J.R., and Bushman, F. (2002). HIV-1
690 Integration in the Human Genome Favors Active Genes and Local Hotspots. Cell *110*, 521–529.
691 https://doi.org/10.1016/S0092-8674(02)00864-4.

692 47. Tchasovnikarova, I.A., Timms, R.T., Matheson, N.J., Wals, K., Antrobus, R., Göttgens, B., Dougan,
693 G., Dawson, M.A., and Lehner, P.J. (2015). Epigenetic silencing by the HUSH complex mediates
694 position-effect variegation in human cells. Science *348*, 1481–1485.
695 https://doi.org/10.1126/science.aaa7227.

696 48. Yurkovetskiy, L., Guney, M.H., Kim, K., Goh, S.L., McCauley, S., Dauphin, A., Diehl, W.E., and
697 Luban, J. (2018). Primate immunodeficiency virus proteins Vpx and Vpr counteract
698 transcriptional repression of proviruses by the HUSH complex. Nat. Microbiol. *3*, 1354–1361.
699 https://doi.org/10.1038/s41564-018-0256-x.

700 49. Pollack, R.A., Jones, R.B., Pertea, M., Bruner, K.M., Martin, A.R., Thomas, A.S., Capoferri, A.A.,
701 Beg, S.A., Huang, S.H., Karandish, S., et al. (2017). Defective HIV-1 Proviruses Are Expressed and
702 Can Be Recognized by Cytotoxic T Lymphocytes, which Shape the Proviral Landscape. Cell Host
703 Microbe *21*, 494-+. https://doi.org/10.1016/j.chom.2017.03.008.

704 50. Collora, J.A., Liu, R., Pinto-Santini, D., Ravindra, N., Ganoza, C., Lama, J.R., Alfaro, R., Chiarella, J.,
705 Spudich, S., Mounzer, K., et al. (2022). Single-cell multiomics reveals persistence of HIV-1 in
706 expanded cytotoxic T cell clones. Immunity *55*, 1013-1031.e7.
707 https://doi.org/10.1016/j.immuni.2022.03.004.

708 51. Kinloch, N.N., Shahid, A., Dong, W., Kirkby, D., Jones, B.R., Beelen, C.J., MacMillan, D., Lee, G.Q.,
709 Mota, T.M., Sudderuddin, H., et al. (2023). HIV reservoirs are dominated by genetically younger
710 and clonally enriched proviruses. mBio *14*, e0241723. https://doi.org/10.1128/mbio.02417-23.

711 52. Gunst, J.D., Pahus, M.H., Rosás-Umbert, M., Lu, I.-N., Benfield, T., Nielsen, H., Johansen, I.S.,
712 Mohey, R., Østergaard, L., Klastrup, V., et al. (2022). Early intervention with 3BNC117 and
713 romidepsin at antiretroviral treatment initiation in people with HIV-1: a phase 1b/2a,
714 randomized trial. Nat. Med. *28*, 2424–2435. https://doi.org/10.1038/s41591-022-02023-7.

715 53. Armani-Tourret, M., Gao, C., Hartana, C.A., Sun, W., Carrere, L., Vela, L., Hochroth, A., Bellefroid,
716 M., Sbrolla, A., Shea, K., et al. (2024). Selection of epigenetically privileged HIV-1 proviruses
717 during treatment with panobinostat and interferon-α2a. Cell, S0092-8674(24)00105-3.
718 https://doi.org/10.1016/j.cell.2024.01.037.

719 54. Shan, L., Deng, K., Gao, H.B., Xing, S.F., Capoferri, A.A., Durand, C.M., Rabi, S.A., Laird, G.M., Kim,
720 M., Hosmane, N.N., et al. (2017). Transcriptional Reprogramming during Effector-to-Memory
721 Transition Renders CD4(+) T Cells Permissive for Latent HIV-1 Infection. Immunity *47*, 766-+.
722 https://doi.org/10.1016/j.immuni.2017.09.014.

723 55. Hataye, J.M., Casazza, J.P., Best, K., Liang, C.J., Immonen, T.T., Ambrozak, D.R., Darko, S., Henry,
724 A.R., Laboune, F., Maldarelli, F., et al. (2019). Principles Governing Establishment versus Collapse
725 of HIV-1 Cellular Spread. Cell Host Microbe *26*, 748-763.e20.
726 https://doi.org/10.1016/j.chom.2019.10.006.

727 56. Zhang, Z., Nikolai, B.C., Gates, L.A., Jung, S.Y., Siwak, E.B., He, B., Rice, A.P., O'Malley, B.W., and
728 Feng, Q. (2017). Crosstalk between histone modifications indicates that inhibition of arginine
729 methyltransferase CARM1 activity reverses HIV latency. Nucleic Acids Res. *45*, 9348–9360.
730 https://doi.org/10.1093/nar/gkx550.

731 57. Huang, D.W., Sherman, B.T., and Lempicki, R.A. (2009). Systematic and integrative analysis of
732 large gene lists using DAVID bioinformatics resources. Nat. Protoc. *4*, 44–57.
733 https://doi.org/10.1038/nprot.2008.211.

734

735

736 ## Figures

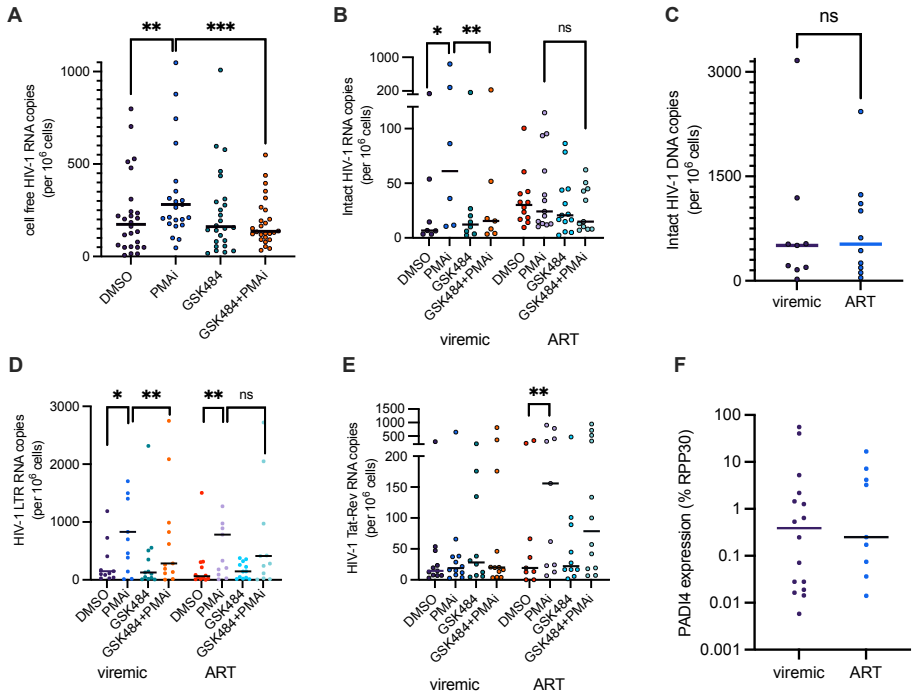

737

738 **Fig 1: PADI4 stimulates HIV-1 transcription after cell stimulation in cells from viremic people with**
739 **HIV-1.**

740 (A) Extracellular HIV-1 RNA with PMAi and GSK484 treatments from entire cohort (n=31, study
741 participant characteristics in Table S1).
742 (B) Intracellular cell-associated HIV-1 RNA in the cohort stratified into in viremic and long-term ART
743 suppressed groups.
744 (C) Intact HIV-1 proviral reservoir from the two groups measured by IPDA.
745 (D-E) HIV-1 5´LTR RNA (D) and Tat-Rev (E) quantified in viremic (n=14) and long-term ART suppressed
746 groups (n=17).
747 (F) PADI4 expression in the two groups normalised to RPP30.
748 All statistical tests shown are Wilcoxon matched-pairs signed rank test * p<0.05, ** p<0.01, ***
749 p<0.001.

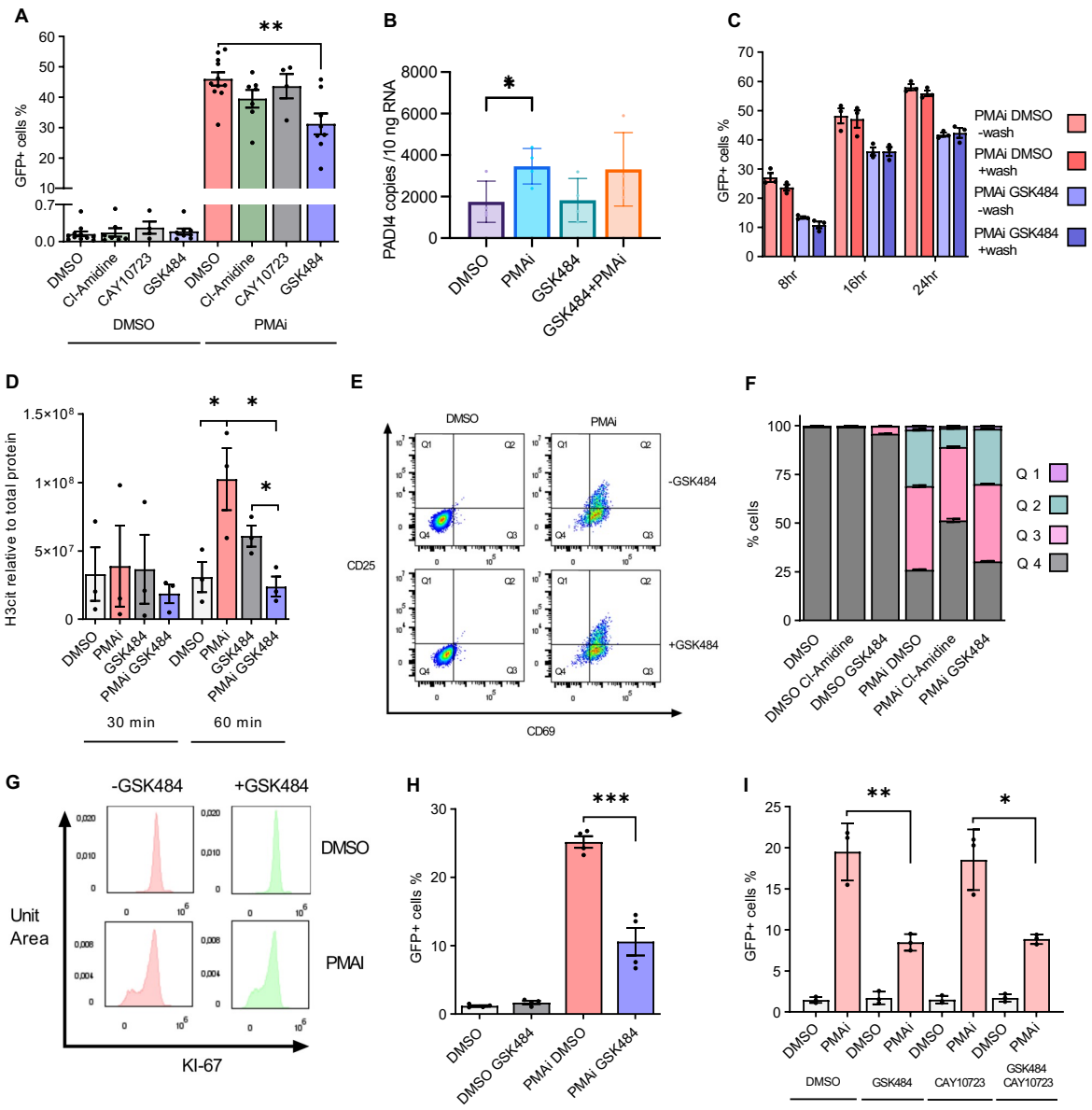

Fig 2 PADI4 facilitates HIV-1 transcription after cell stimulation in cell models.

(A) J-Lat 5A8 cells treated with PADI inhibitors and PMAi activation. GFP measured by flow cytometry (n=8-11).

(B) PADI4 expression in 5A8 measured by ddPCR under PMAi and GSK484 treatment (n=4).

(C) Time course of 5A8 under PMAi and GSK484 treatment and flow cytometry quantification of GFP. Cells were washed and resuspended in new media without drugs after 1 h (n=3).

(D) H3cit (R2, R8, R17 residues) quantification by immunoblot in 5A8 with PMAi and GSK484 treatment at two early timepoints (n=3).

(E) T cell activation phenotype for 5A8 as measured by flow cytometry. CD69 appears early during T cell activation, CD25 appears late during late T cell activation.

(F) T cell activation of 5A8 after 24 h with different PADI4 inhibitors and PMAi activated cells (n=3).

762 (G) Staining with proliferation marker KI-67 of 5A8 treated for 24 h with PMAi and GSK484
763 (H) Polyclonal K562-Lat treated with PMAi and GSK484 for 24 h and quantified with flow cytometry
764 (n=4).
765 (I) Polyclonal K562-Lat treated with PMAi, GSK484, and CAY10723 for 24 h and quantified with
766 flow cytometry (n=3)
767 Data is shown as mean ± SEM. Statistical tests shown are unpaired T tests * $p<0.05$, ** $p<0.01$, ***
768 $p<0.001$.
769

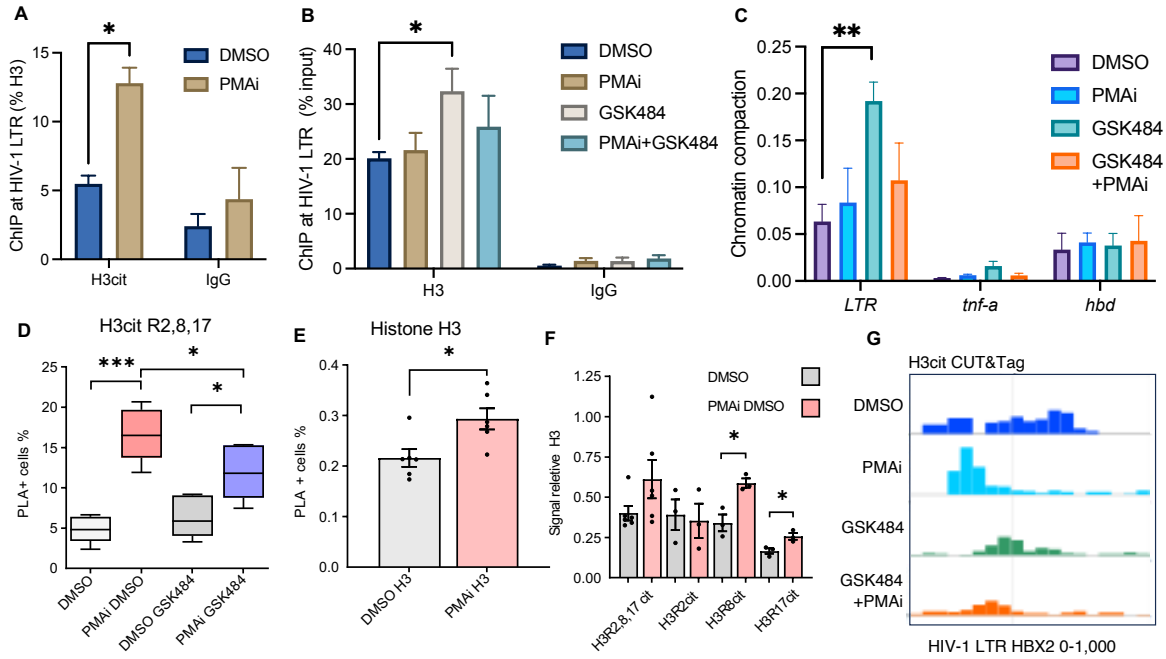

Fig 3: Citrullinated histone H3 at the HIV-1 provirus stimulated latency reversal.

(A) H3cit signal at a HIV LTR locus in 5A8 cells, measured by ChIP-qPCR.

(B) H3 signal at the HIV LTR locus in 5A8 cells, measured by ChIP-qPCR.

(C) Chromatin compaction at the HIV LTR and TNFα. Quantified with chromatin accessibility kit

(D) Quantification of H3cit at the HIV-1 LTR in 5A8 cells under PMAi and GSK484 treatment using PLA-ZFP assay (n=6).

(E) Quantification of Histone H3 at HIV-1 LTR in 5A8 cells under PMAi treatment using PLA-ZFP assay (n=6).

(F) Quantification of different H3cit residues with PLA-ZFP in 5A8 relative to H3 (n=3-6)

(G) CUT&Tag seq view of total H3cit after 24 h treatment over the HIV-1 LTR. Grey line indicates TSS.

Data is shown as mean ± SEM. Statistical tests shown are unpaired T tests *= <0.05 *= <0.01 *= <0.001

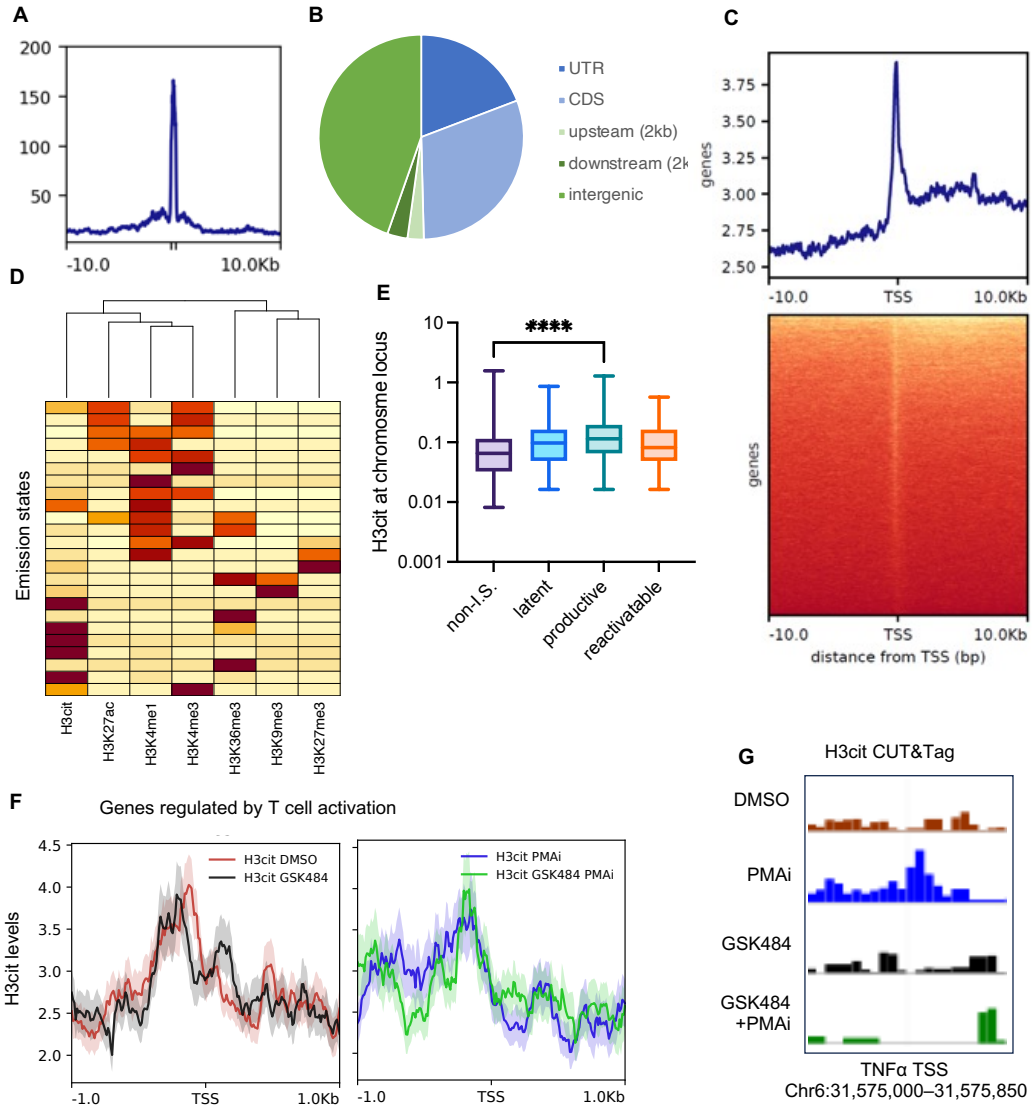

Fig 4: Genome-wide H3cit levels are stable at promoters in 5A8 with HIV-1 preferentially integrating into H3cit chromatin.

(A) CUT&Tag peak width profile.

(B) Relative enrichment of peaks in genic and non-genic regions.

(C) Metagene plot for DMSO treated 5A8 samples

(D) ChromHMM analysis showing similarity between chromatin marks.

(E) Quantification of H3cit mapped onto known proviral integration sites with corresponding proviral activation.

(F) Metagene plot with a gene set regulated by T cell activation ("GSE13738 Resting vs TCR activated CD4 T cell").

(G) Genome browser view of the H3cit signal over the TNFα promoter region. Grey line indicates the TSS.

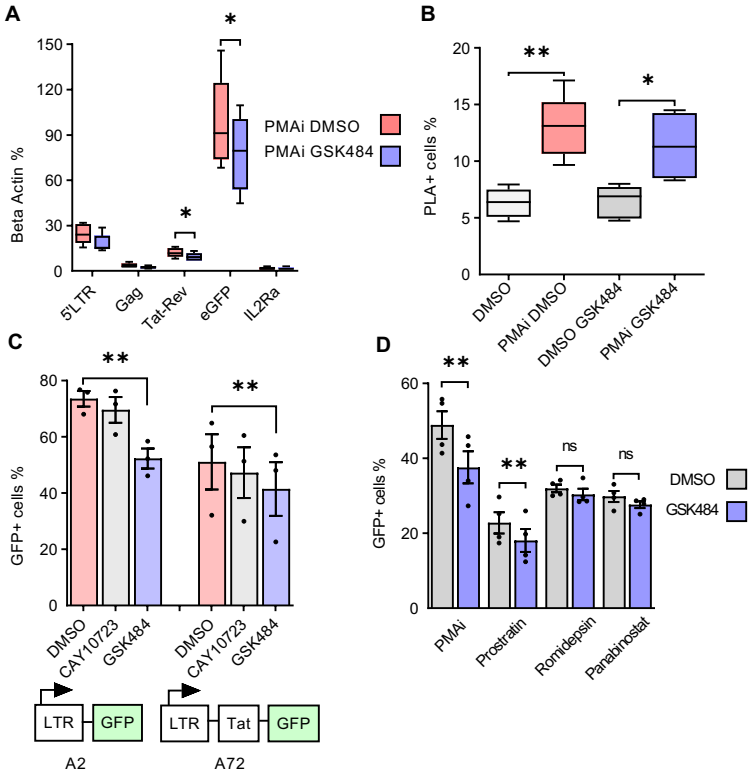

Fig 5: *de novo* H3cit has a general effect on HIV-1 transcription, but not through Tat or acetylation.

(A) RT-qPCR quantification of short initiated (5´-LTR), early elongated unspliced (Gag), multiply spliced (Tat-Rev), and late elongated (GFP) transcripts in 5A8 treated with PMAi and GSK484. Statistical tests shown are paired T tests *p<0.05 (n=5).

(B) Levels of Tat at the HIV-1 promoter in 1C10 cells with PMAi and GSK484 using PLA-ZFP assay. Statistical tests shown are unpaired T tests * p<0.05, ** p<0.01, *** p<0.001 (n=6).

(C) HIV-1 transcription of in Tat negative J-Lat A2 and Tat positive A72 cells treated with PMAi and PADI inhibitors, measured by flow cytometry. Statistical tests shown are paired T tests * p<0.05, ** p<0.01, *** p<0.001 (n=3).

(D) 5A8 cells treated with PMAi and other latency reversal agents and GSK484 (n=4).

Data is shown as mean ± SEM.

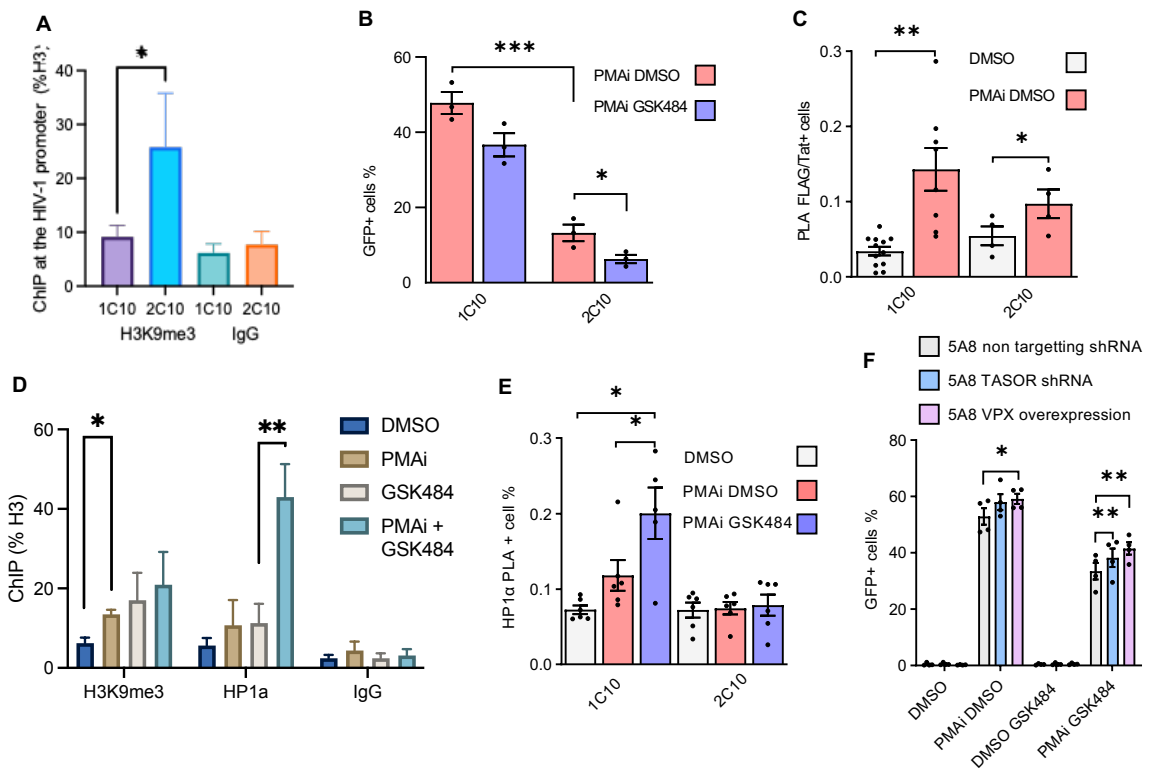

Fig 6: Heterochromatin forms over the HIV-1 provirus in the absence of H3cit.

(A) H3K9me3 at the HIV-1 locus in 1C10 (ZFP) and 2C10 (ZFP-KRAB) cells measured by ChIP-qPCR. Statistical tests shown are unpaired T tests * p<0.05 (n=3).

(B) 1C10 and 2C10 cell HIV-1 transcription with PMAi and GSK484 treatment. Statistical tests shown are unpaired T tests * p<0.05, ** p<0.01, *** p<0.001 (n=3).

(C) Tat proximity to HIV-1 promoter in 1C10 and 2C10 cells with PMAi treatment. Statistical tests shown are paired T tests * p<0.05, ** p<0.01 (n=6-12).

(D) H3K9me3 and HP1α levels at the readth locus in 1C10 measured by ChIP-qPCR

(E) HP1α proximity to the HIV-1 promoter in 1C10 and 2C10 cells with PMAI and PMAi and GSK484 treatment (n=5-6).

(F) GFP quantification by flow cytometry of 5A8 TASOR RNAi knockdown and 5A8 VPX overexpression cells (n=3).

Data is shown as mean ± SEM.